

Research of the Anti-Penetration Mechanism for Titanium Alloys Armor Based on 3D Optical Scanning Technology

Yumeng Xia^{1,2}, Qunbo Fan^{1,2,a*}, Ruihua Gao^{1,2}, Guoju Li^{1,2}, Lirui Huo^{1,2}, Yipeng Zhang^{1,2}

¹School of Materials Science and Engineering, Beijing Institute of Technology, Beijing 100081 P. R. China

²National Key Laboratory of Science and Technology on Materials under Shock and Impact, Beijing 100081 P. R. China

^afanqunbo@bit.edu.cn

Keywords: Titanium alloy, anti-penetration mechanism, 3D optical scanning.

Abstract. To reveal the anti-penetration mechanism of titanium alloys armor quantitatively, the volumes of the front crater region, the ductile hole-enlargement region, as well as the back caving region of Ti-6Al-4V alloy and β 20C alloy were measured via 3D Optical scanning technology. The experimental results show that β 20C alloy, of which the volume fraction of ductile hole-enlargement region is 51%, 10% larger than that of Ti-6Al-4V alloy, presents a better ballistic performance. It is found that the ballistic performance is closely related to the volume of ductile hole-enlargement region and a relatively larger ductile hole is beneficial to improve the ballistic performance. However, the ballistic performance shows no improvement with increasing the volume of front crater region.

Introduction

For a better ballistic performance of light armors, titanium alloys have a wide prospect for the special properties, such as the low density and high strength-to-weight ratio. However, little research has been done in the ballistic performance and anti-penetration mechanism of titanium alloys[1,2].

When it comes to anti-penetration mechanism, people usually focus on the macroscopic appearance[3,4], such as the depth and diameter of the penetration, but scarcely on the quantitative relation of the front crater region, the ductile hole-enlargement region and the back caving region. By 3D optical scanning methods, the volumes of the three regions of the penetration were calculated based on two kinds of titanium alloys, the most widely used Ti-6Al-4V alloy and β 20C alloy. β 20C alloy is a new type of titanium alloy designed by Beijing Institute of Technology. Therefore the anti-penetration mechanism was expected to be characterized quantitatively by comparing the volumes of these regions.

Experimental

Materials

The composition of β 20C alloy is listed in Table 1. Ti-6Al-4V alloy was used as received and β 20C alloy was used after a heat treatment of 920°C/0.5h/FC. Target specimens were machined in the dimension of 100mm×100mm×40mm.

Table 1 Composition of β 20C alloy

Element	Ti	Al	Mo	Zr	Sn	Cr	Fe
Content [Wt%]	Bal.	5.0~6.5	3.5~4.5	3.5~4.5	2.5~3.5	1.5~3.0	0.2~0.7

Experimental Methods

Ballistic Impact Tests

The projectile used in this test was 105mm armor-piercing bullet penetrating at normal incidence, as shown in Fig.1. The initial velocity of the projectile is about 1335m/s. In addition, the 40mm thick titanium alloy target specimen was placed in front of the 60mm thick 603 armor steel plate without space.

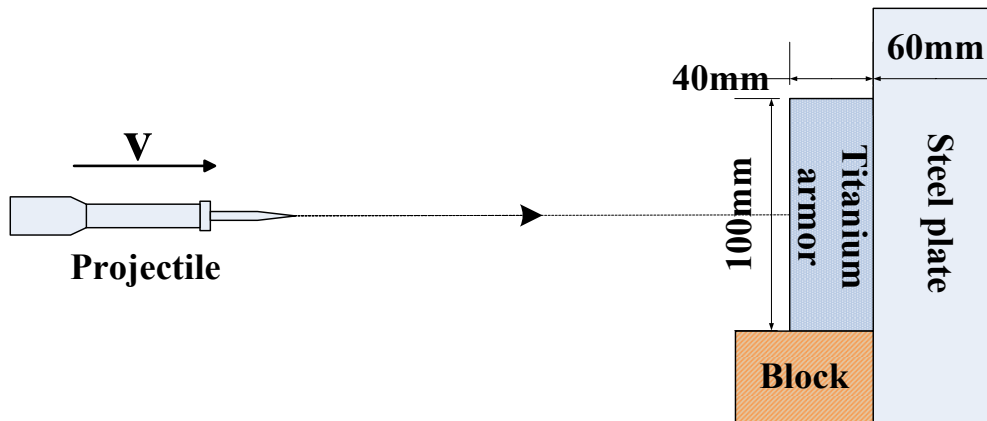


Fig. 1 Schematic diagram of the ballistic impact test system

3D Optical Scanning Experiment

The 3D shape of the bullet hole in the target was measured by scanning the target specimen with Win3DD non-contact passive 3D optical scanner. Fig.2 shows the principle of the 3D scanner schematically. The multimedia white light projector (DLP) projects a light pattern of parallel stripes onto a three-dimensionally shaped surface. Seen from different viewpoints, the pattern appears geometrically distorted due to the surface shape of the object and is photographed by monochrome digital cameras (CCD). The displacement of the stripes allows an exact retrieval of the 3D coordinates of any details on the object's surface.

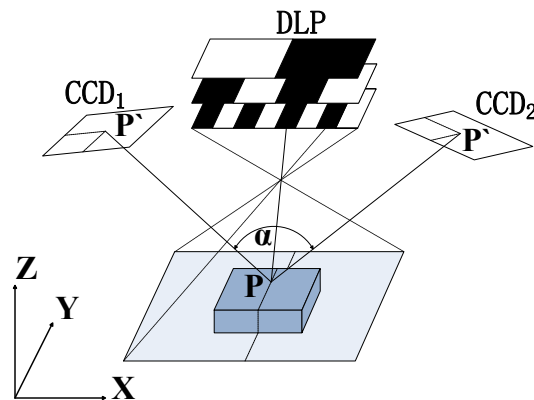


Fig.2 Schematic diagram of the principle of the 3D optical scanner

Results & discussion

Ballistic performance

The sections of the bullet hole on the rear panel are shown in Fig.3. As is well known, a common method to evaluate the ballistic performance is measuring the depth of penetration of the rear panel (DOP) and calculating the mass efficiency coefficient (N), which is expressed as:

$$N = \frac{\rho_1(L_1+L_2)}{\rho_2d} \quad (1)$$

Where ρ_1 is the density of the rear panel; ρ_2 is the density of the titanium alloy plate; L_1 is the depth of the penetration of RHA at normal incidence ($L_1=65\text{mm}$); L_2 is the depth of the penetration of the rear panel; d is the thickness of the titanium alloy plate ($d=40\text{mm}$). The ballistic impact test results are listed in Table 2.

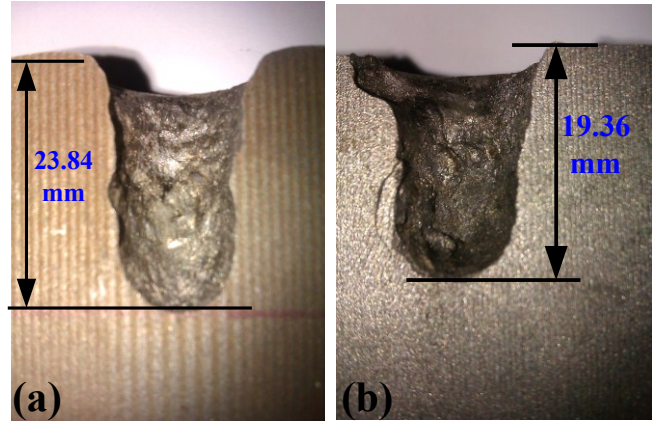


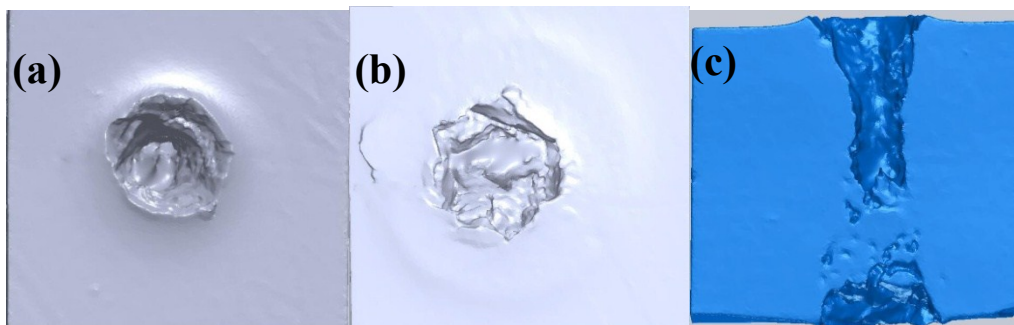
Fig.3 The sections of bullet hole on the rear panel (a) Front panel is Ti-6Al-4V (b) Front panel is β 20C

Armor	DOP[mm]	N
Ti-6Al-4V	23.84	1.78
β 20C	19.36	1.93

It can be seen that the N value of β 20C is calculated to be 1.93, which shows an improvement of 8.4% over that of Ti-6Al-4V. Thus, the ballistic performance of β 20C is better if compared with that of Ti-6Al-4V.

Observation and quantitative characterization of bullet hole based on 3D optical scanning

Fig.4 shows the macroscopic appearance of the bullet hole on Ti-6Al-4V and β 20C alloy target plates obtained by 3D optical scanning. In Fig.4 (a) and (d), the front side of Ti-6Al-4V target plate presents a larger reverse protrusion than that of β 20C. Being restrained by 603 armor steel plate, the backside of β 20C target plate presents an obvious annular hump compared with that of Ti-6Al-4V, as shown in Fig.4 (b) and (e). By comparing Fig.4 (c) with (f), it is obviously noticed that there is a metal blocking in the bullet hole of Ti-6Al-4V plate, while β 20C plate has a continuous and open bullet hole. It is because the adiabatic shear makes the temperature exceed the melting point of Ti-6Al-4V. Subsequently the solidified metal is jammed in the bullet hole.



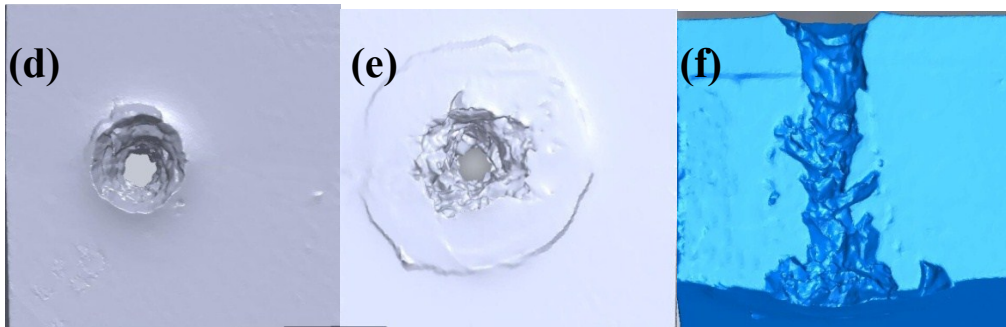


Fig.4 The macroscopic appearance of the bullet hole on titanium alloy target
 (a)Front side of Ti-6Al-4V target (b) Backside of Ti-6Al-4V target (c) Section of bullet hole on Ti-6Al-4V target (d) Front side of β 20C target (e) Backside of β 20C target (f) Section of the bullet hole on β 20C target

Furthermore, seen from the sections of the bullet hole (Fig.4 (c) and (f)), it is found that there is a significant difference in the wall appearance of the bullet hole between the two target plates. The wall of Ti-6Al-4V is relatively smooth and symmetrical, indicating that it is slightly easier for the bullet to penetrate the target plate. Nevertheless, the wall of β 20C is quite rough, irregular and less symmetrical, which indicates that the bullet was hindered so seriously during the penetration.

By 3D inverse operation, the 3D solid model of the bullet holes on Ti-6Al-4V and β 20C target plates were obtained, as shown in Fig.5 (a) and (b). The volumes and volume fractions of the front crater region, the ductile hole-enlargement region, as well as the back caving region were measured and summarized respectively in Table 3. It is necessary to state that the blocking part of the ductile hole-enlargement region of Ti-6Al-4V (Fig.5 (a)) was included when calculating the volume of the ductile hole-enlargement region. It can be clearly seen that the volume fraction of the ductile hole-enlargement region is larger than the other regions of the bullet hole for both Ti-6Al-4V and β 20C. Further study shows that the volume fraction of the ductile hole-enlargement of β 20C, which is about 51%, is larger than that of Ti-6Al-4V, 41%. Moreover, the volume fraction of the front crater region of β 20C (about 15%) is less than that of Ti-6Al-4V (about 26%). However, the volume fractions of the back caving region of these two alloys are similar, approached to 33%.

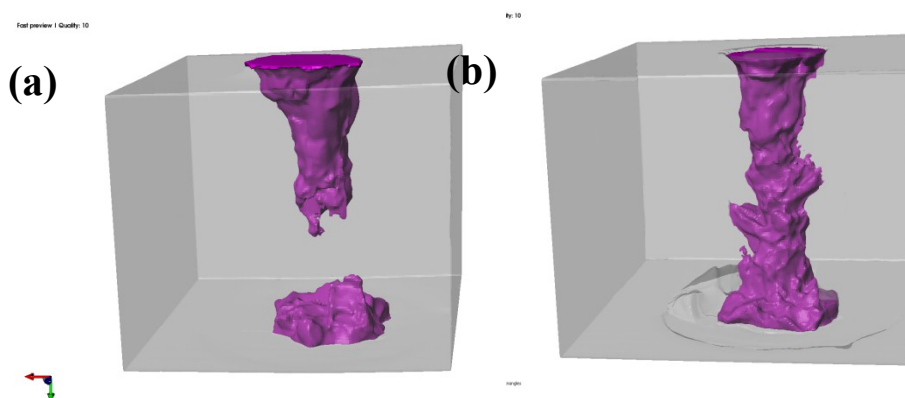
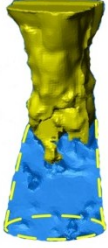
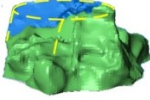
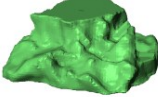


Fig.5 The 3D solid shape of the bullet hole
 (a) Ti-6Al-4V (b) β 20C

Table 3 The volume fraction and 3D solid shape of each region of the bullet hole

	Ti-6Al-4V			β 20C		
	3D Solid Shape	Volume [mm ³]	Volume Fraction [%]	3D Solid Shape	Volume [mm ³]	Volume Fraction [%]
The front crater region		900	26		480	15
The ductile hole-enlargement region		1400	41		1700	51
The back caving region		1100	33		1100	34

(Remark: the blue part surrounded by the dash line is the melting metal that blocks the bullet hole)

As the target metal flowed radially on the transience of the bullet impact onto the target, also called the front cratering period, the energy of the bullet was slightly consumed. Therefore, the ballistic performance has no improvement with a larger front crater region. However, there was a strong interaction between the bullet and the target during the ductile hole-enlargement period so that a rough bullet-hole wall helps to enlarge the volume of the ductile hole-enlargement region and contributes to enhancing the ballistic performance. It might be mentioned that during the later period of penetration, the ballistic performance was expected to get improved because of the restraint on the target from the rear penal. Whereas the volume fractions of the back caving region of the two alloys are close, and its effect on the ballistic performance needs further study.

Conclusions

1) The 3D solid models of the titanium plates after penetration and the bullet hole are obtained via 3D optical scanning and the inverse operation, respectively.

2) β 20C alloy has an outstanding ballistic performance compared with Ti-6Al-4V alloy. Its volume fraction of the ductile hole-enlargement region reaches 51%, 10% larger than that of Ti-6Al-4V. In addition, the volume fraction of the ductile hole-enlargement region is larger than of the front crater region and the back caving region respectively.

3) In the current test conditions, the ductile hole-enlargement region shows an important influence on the ballistic performance. The larger the ductile hole-enlargement region is, the better the ballistic performance is. However, the ballistic performance does not become improved with a larger volume fraction of the front crater region, and the effects of the back caving region needs further study.

Acknowledgements

We gratefully acknowledge the financial support of the program for New Century Excellent Talents in University (NCET-12-0051).

References

- [1] D.G. Lee, Y.G. Kim, D.H. Nam, S.M. Hur, S. Lee, Dynamic deformation behavior and ballistic performance of Ti–6Al–4V alloy containing fine α_2 (Ti₃Al) precipitates, *J. Materials Science and Engineering: A*. 391(2005) 221-234.
- [2] S.H. Li, D.W. Shen, K. Sun, C.W. Tan, F.C. Wang, S.S. Feng, Damage Behavior of Crater and Microstructure Evolution of Ti-6Al-4V Alloy, *J. Rare Metal Materials and Engineering*. 42(2013)1703-1706.
- [3] Sherman D, Impact failure mechanisms in alumina tiles on finite thickness support and the effect of confinement, *J. International Journal of Impact Engineering*. 24(2000) 313-328.
- [4] C. Miao, J.N. Liu, T. Zhong, S.T. Li, H.L. W, W.L. Yang, Thickness effect of titanium alloy plates against 12.7 mm API, *J. Ordnance Material Science and Engineering*. 35(2012)68-70.